frontiers | Frontiers in Astronomy and Space Sciences

TYPE Original Research
PUBLISHED 09 January 2024
DOI 10.3389/fspas.2023.1294449

OPEN ACCESS

EDITED BY
Renee Ludlam,
Wayne State University, United States

REVIEWED BY
Alice Borghese,
Instituto de Astrofisica de Canarias, Spain
Silvia Zane,
University College London,
United Kingdom

*CORRESPONDENCE
J. A. J. Alford,
alford@nyu.edu

RECEIVED 14 September 2023
ACCEPTED 06 December 2023
PUBLISHED 09 January 2024

CITATION
Alford JAJ, Younes GA, Wadiasingh Z, Abdelmaguid M, An H, Bachetti M, Baring MG, Beloborodov A, Chen AY, Enoto T, García JA, Gelfand JD, Gotthelf EV, Harding AK, Hu C-P, Jaodand AD, Kaspi V, Kim C, Kouveliotou C, Kuiper L, Mori K, Nynka M, Park J, Stern D, Valverde J and Walton DJ (2024), The high energy X-ray probe (HEX-P): magnetars and other isolated neutron stars.
Front. Astron. Space Sci. 10:1294449.
doi: 10.3389/fspas.2023.1294449

The high energy X-ray probe (HEX-P): magnetars and other isolated neutron stars

J. A. J. Alford[1]*, G. A. Younes[2], Z. Wadiasingh[3,4,5], M. Abdelmaguid[1], H. An[6], M. Bachetti[7], M. G. Baring[8], A. Beloborodov[9], A. Y. Chen[10], T. Enoto[11], J. A. García[12], J. D. Gelfand[1], E. V. Gotthelf[9], A. K. Harding[13], C-P. Hu[14], A. D. Jaodand[15], V. Kaspi[16], C. Kim[6], C. Kouveliotou[2], L. Kuiper[17], K. Mori[9], M. Nynka[18], J. Park[6], D. Stern[19], J. Valverde[20] and D. J. Walton[21]

[1]NYU Abu Dhabi, Abu Dhabi, United Arab Emirates, [2]Department of Physics, The George Washington University, Washington, DC, United States, [3]Astrophysics Science Division, NASA/GSFC, Greenbelt, MD, United States, [4]Department of Astronomy, University of Maryland, College Park, MD, United States, [5]Center for Research and Exploration in Space Science and Technology, NASA/GSFC, Greenbelt, MD, United States, [6]Department of Astronomy and Space Science, Chungbuk National University, Cheongju, Republic of Korea, [7]INAF-Osservatorio Astronomico di Cagliari, Selargius, Italy, [8]Department of Physics and Astronomy—MS 108, Rice University, Houston, TX, United States, [9]Columbia Astrophysics Laboratory, Columbia University, New York, NY, United States, [10]Physics Department and McDonnell Center for the Space Sciences, Washington University in St. Louis, St. Louis, MO, United States, [11]Extreme Natural Phenomena RIKEN Hakubi Research Team, Cluster for Pioneering Research, RIKEN, Wako, Saitama, Japan, [12]X-ray Astrophysics Laboratory, NASA Goddard Space Flight Center, Greenbelt, MD, United States, [13]Theoretical Division, Los Alamos National Laboratory, Los Alamos, NM, United States, [14]Department of Physics, National Changhua University of Education, Changhua, Taiwan, [15]Division of Physics, California Institute of Technology, Pasadena, CA, United States, [16]Department of Physics, McGill University, 3600 rue University, Montreal, QC, Canada, [17]SRON-Netherlands Institute for Space Research, Leiden, Netherlands, [18]Kavli Institute For Astrophysics and Space Research, Massachusetts Institute of Technology, Cambridge, MA, United States, [19]Jet Propulsion Laboratory, California Institute of Technology, Pasadena, CA, United States, [20]Department of Physics and Center for Space Sciences and Technology, University of Maryland Baltimore County, Baltimore, MD, United States, [21]Centre for Astrophysics Research, University of Hertfordshire, College Lane, Hatfield, United Kingdom

The hard X-ray emission from magnetars and other isolated neutron stars remains under-explored. An instrument with higher sensitivity to hard X-rays is critical to understanding the physics of neutron star magnetospheres and also the relationship between magnetars and Fast Radio Bursts (FRBs). High sensitivity to hard X-rays is required to determine the number of magnetars with hard X-ray tails, and to track transient non-thermal emission from these sources for years post-outburst. This sensitivity would also enable previously impossible studies of the faint non-thermal emission from middle-aged rotation-powered pulsars (RPPs), and detailed phase-resolved spectroscopic studies of younger, bright RPPs. The High Energy X-ray Probe (HEX-P) is a probe-class mission concept that will combine high spatial resolution X-ray imaging (<5 arcsec half-power diameter (HPD) at 0.2–25 keV) and broad spectral coverage (0.2–80 keV) with a sensitivity superior to current facilities (including XMM-Newton and NuSTAR). HEX-P has the required timing resolution to perform follow-up observations of sources identified by other facilities and positively identify candidate pulsating neutron stars. Here we discuss how HEX-P is ideally

suited to address important questions about the physics of magnetars and other isolated neutron stars.

KEYWORDS

X-ray sources, HEX-P, pulsars, magnetars, neutron stars, spectra Frontiers

1 Introduction

Massive stars ($\gtrsim 8\ M_\odot$) end their lives in spectacular supernovae, leaving behind either a neutron star (NS) or a black hole (BH) (Heger et al., 2003). NSs are very compact (having masses of ≈1.4 $M_\odot$ and radii of ≈10 km), and isolated NSs typically have strong magnetic fields ($B \gtrsim 10^{12}$ G, though see the discussion of central compact objects (CCOs) below). The telltale sign for the existence of an NS is the detection of their spin ephemerides, most notably their spin periods P and, if multi-epoch observations exist, their period derivatives $\dot{P}$. These two observational properties can be used to estimate three key fundamental physical scales under the assumption of a rotating dipole magnet in vacuum (Figure 1): 1) rotational energy loss $|\dot{E}| \propto \dot{P}/P^3$, 2) characteristic spin-down age $\tau_{\rm char} = P/2\dot{P}$, and 3) surface dipolar magnetic field strength $B_{\rm dip} \propto \sqrt{P\dot{P}}$.

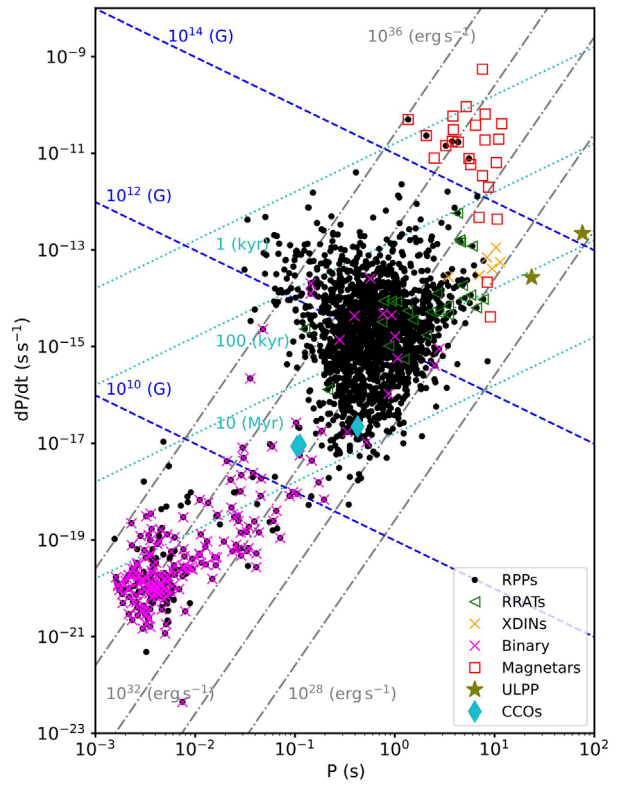

FIGURE 1
Pulsar period period-derivative diagram highlighting the range of neutron star classes. Note lines of constant rotational energy loss $|\dot{E}| \propto \dot{P}/P^3$, characteristic spin-down age $\tau_{\rm char} = P/2\dot{P}$, and surface dipolar magnetic field strength $B_{\rm dip} \propto \sqrt{P\dot{P}}$. Data are from the ATNF pulsar catalog version 1.65 (Manchester et al., 2005).

Since their discovery, a number of unique classes of isolated NSs (INSs) have been identified through differences in their broadband emission characteristics, location/environment, and timing behavior. The most common of the INS population are the rotation-powered pulsars (RPPs), aptly named given that their large spin-down power $\dot{E}$ far exceeds their total radiative luminosity. Then, there are the magnetars, which possess periods typically in the range of about 1–15 s and large spin-down rates ($\dot{P} \sim 10^{-11}$ s s^{-1}), thus occupying a unique space in the P-$\dot{P}$ diagram (Figure 1, red squares). Assuming magnetic dipole braking, the magnetar timing properties translate to dipole field strengths of the order of 10^{14} G (two orders of magnitude larger than RPPs, Kouveliotou et al., 1998; Kouveliotou et al., 1999; Kaspi et al., 2003), average spin-down ages of 10^4 years (confirmed through the association of a few with young, X-ray bright supernova remnants (SNRs), see, e.g., Vasisht and Gotthelf 1997), and low spin-down power $|\dot{E}| \sim 10^{32}$ erg s^{-1} (Olausen and Kaspi, 2014). Despite the latter, magnetars are observed as hot thermal emitters with surface thermal temperatures $kT \approx 0.5$ keV (factors of ~2 larger than young RPPs; see, e.g., Figure 1 of Olausen and Kaspi, 2014), and X-ray luminosities $\gtrsim 10^{33}$ erg s^{-1}. Hence, magnetar radiative power is attributed to the decay of their extreme external and internal B-fields (Thompson and Duncan, 1995; Kaspi and Beloborodov, 2017).

Then there are the dozen known CCOs, which are perhaps the least understood class of INSs (De Luca, 2017). The three CCOs with measured spin ephemerides are indicated with blue diamonds in Figure 1. These point-like X-ray sources are found in young X-ray bright SNRs, and lack both emission at other wavelengths and any associated pulsar wind nebula. While there are relatively few identified CCOs, their locations in young SNRs suggests that they may represent a significant fraction of NS births. CCOs are also known as "anti-magnetars," since some of them have the smallest spin-down-measured dipole magnetic field strengths among all known young NSs (Gotthelf et al., 2013), at odds with their relatively bright thermal X-ray emission.

X-ray dim isolated NSs (XDINSs, yellow crosses in Figure 1) constitute a population with observational characteristics that do not quite fit the above classes. They are nearby (within a few hundred parsecs, Kaplan, 2008), radio-quiet (but see Rigoselli et al., 2019), yet thermally-emitting with surface temperatures in the range of 45–110 eV and luminosities $L_{\rm X} < 10^{32}$ erg s^{-1}. This emission is pulsed at a spin-period of a few seconds, while slowing down with a rate of $\dot{P} \approx 10^{-14}$ s s^{-1}, implying $B_{\rm dip} \sim 10^{13}$ G, $\tau \gtrsim 1$ Myr, and an average $\dot{E} \sim 5 \times 10^{30}$ erg s^{-1}. Given their small $|\dot{E}|$ compared to their surface thermal emission, XDINS are thought to be powered by their relatively large B-fields, akin to magnetars, which are thought to be their younger counterparts according to magneto-thermal evolutionary models.

Recently, a new class of long-period radio-emitting NSs have been discovered with spin periods of tens of seconds and relatively large spin-down rates (Tan et al., 2018; Caleb et al., 2022; green stars

in Figure 1). Their dipole-inferred fields are comparable to those of magnetars and XDINs. They are also relatively nearby with distances of the order of 1 kpc, yet deep X-ray observations have not detected their high energy counterpart with upper-limits comparable to those of XDINs (Rea et al., 2022; Beniamini et al., 2023). These limits are consistent with the old magnetar interpretation, though how they maintain dipolar-fields of 10^{14} G is less clear (Caleb et al., 2022; Beniamini et al., 2023).

Our understanding of the young INS population has been predominantly shaped by radio and X-ray observations. Radio surveys of large areas of the Galaxy provide understanding of the birth rate and properties of NSs (e.g., Arzoumanian et al., 2002; Faucher-Giguère and Kaspi, 2006), while X-ray observations established several of the above sub-classes, and highlighted the connections among them; e.g., RPPs and CCOs showing magnetar-like bursting and outburst abilities (Gavriil et al., 2008; Archibald et al., 2016b; Rea et al., 2016), the existence of low B-field magnetars (Rea et al., 2010), and bona-fide magnetars with RPP characteristics such as radio emission and pulsar wind nebulae (Camilo et al., 2006; Camilo et al., 2007; Younes et al., 2016). All of these X-ray discoveries have led to several attempts at unifying these sub-classes (Kaspi and Boydstun, 2010), mainly through magneto-thermal evolution models (Viganò et al., 2013; Gourgouliatos et al., 2016). Lastly, in a breakthrough discovery, the long-held view that Fast Radio Bursts (FRBs) might be powered by magnetar activity was confirmed after the detection of an FRB (CHIME/FRB Collaboration et al., 2020; Bochenek et al., 2020) simultaneous with a hard X-ray burst (e.g., Mereghetti et al., 2020; Li et al., 2021) from a Galactic magnetar in outburst (see Zhang (2023) for a review of FRBs).

In this paper, we present the case for the probe-class mission HEX-P as the next-generation X-ray satellite to build upon the legacy of all past and current X-ray satellites, and open up avenues for new discoveries in the timely field of high energy studies of young INSs. A companion paper, Ludlam et al. (in prep.), discusses the power of HEX-P to study neutron stars in low- and high-mass binary systems.

2 Mission design

The High-Energy X-ray Probe (HEX-P; Madsen et al., 2015) is a probe-class mission concept that offers sensitive broad-band coverage (0.2–80 keV) of the X-ray spectrum with exceptional spectral, timing and angular capabilities. It features two high-energy telescopes (HETs) that focus hard X-rays and one low-energy telescope (LET) that focuses lower-energy X-rays. The HET and LET will observe simultaneously, and both telescopes are well suited for timing studies (e.g., periodicity searches), with timing resolution ~1 μs and 1 m. The HEX-P LET and HET will achieve a factor of ~3 and ~10 or better improvements in sensitivity over XMM-EPIC and NuSTAR telescopes in the 0.2–20 and 3–70 keV bands, respectively. These sensitivity improvements are partially due to the high earth orbit (HEO), in contrast to NuSTAR's low earth orbit (LEO).

The LET consists of a segmented mirror assembly coated with Ir on monocrystalline silicon that achieves a half power diameter of 3.5″, and a low-energy DEPFET detector, of the same type as the Wide Field Imager (WFI; Meidinger et al., 2020) onboard Athena (Nandra et al., 2013). It has 512 × 512 pixels that cover a field of view of 11.3′ × 11.3′ (1.32″/pixel). It has an effective passband of 0.2–25 keV, and a full frame readout time of 2 m, which can be operated in a 128 and 64 channel window mode for higher count-rates to mitigate pile-up and faster readout. Pile-up effects remain below an acceptable limit of ~1% for fluxes up to ~100 mCrab in the smallest window configuration. Excising the core of the point spread function (PSF), a common practice in X-ray astronomy, will allow for observations of brighter sources, with a typical loss of up to ~60% of the total photon counts.

The HET consists of two co-aligned telescopes and detector modules. The optics are made of Ni-electroformed full shell mirror substrates, leveraging the heritage of XMM-Newton (Jansen et al., 2001), and coated with Pt/C and W/Si multilayers for an effective passband of 2–80 keV. The high-energy detectors are of the same type as flown on NuSTAR (Harrison et al., 2013), and they consist of 16 CZT sensors per focal plane, tiled 4 × 4, for a total of 128 × 128 pixel spanning a field of view of 13.4′ × 13.4′.

The broad X-ray passband and superior sensitivity will provide a unique opportunity to study INSs across a wide range of energies, luminosity, and dynamical regimes.

3 Simulations

All the simulations presented here were produced with a set of response files that represent the observatory performance based on current best estimates as of Spring 2023 (see Madsen et al., 2023). The effective area is derived from a ray-trace of the mirror design including obscuration by all known structures. The detector responses are based on simulations performed by the respective hardware groups, with an optical blocking filter for the LET and a Be window and thermal insulation for the HET. The LET background was derived from a GEANT4 simulation (Eraerds et al., 2021) of the WFI instrument, and the HET background was derived from a GEANT4 simulation of the NuSTAR instrument, with both simulations adopting a Lagrange point L1 orbit for HEX-P.

We utilize Xspec version 12.13.0c to simulate point source spectra, implementing HEX-P LET and HET response matrices, ancillary, and background files version v07 (Arnaud, 1996). All simulated spectra are binned to have 5 counts per energy channel. For spectral fitting, we utilize the Cash-statistic (C-stat in Xspec, Cash, 1979), to derive the best fit model parameters and corresponding uncertainties. To assess the goodness of fit, we utilize the goodness command which simulates 1000 spectral realizations from a given model and compares their fit statistic to that of the data; if the data is drawn from the model, or, in other words, the model is a good fit to the data, the fit statistic should lie around the 50% mark.

4 Magnetars

4.1 Persistent broadband X-ray emission

Magnetar persistent emission consists of two components, a thermal emission likely emanating from surface hot-spots with temperatures of ~ 0.4–0.5 keV, and a non-thermal component

with photon index $\Gamma = 0.0$–1.5, i.e., rising in νF_ν, known as the hard X-ray tail. The latter likely originates from inverse Compton scattering of soft photons by relativistic electrons in non-potential magnetospheric loops energized by twists and currents, tied to footpoints whose evolution is driven internally by the crust of the magnetar. Due to the large magnetic fields, the scattering in the magnetosphere is resonant at the electron cyclotron frequency, which is efficient at boosting the photon energies by orders of magnitude relative to the non-resonant case, a process known as Resonant Inverse Compton Scattering (RICS).

Hard X-ray tails were first discovered in 2004 with INTEGRAL and RXTE (Kuiper et al., 2004). Prior to the NuSTAR launch, only a handful of magnetars were detected at energies >10 keV (Kuiper et al., 2006; den Hartog et al., 2008b; den Hartog et al., 2008a; Enoto et al., 2010). NuSTAR, with its superior sensitivity at hard X-rays, has doubled the pool of detected sources, which is currently standing at 10 (e.g., Enoto et al., 2017). The faintest known magnetar hard X-ray tail has a 10–100 keV flux of $\sim 10^{-12}$ erg s^{-1} cm^{-2}; an order of magnitude fainter than detections by NuSTAR predecessors. HEX-P, owing to its superior sensitivity, simultaneous broad-band coverage, and more efficient orbit, will detect magnetar hard X-ray tails an order of magnitude fainter again, and characterize their spectral curvature (i.e., a possible energy dependence of the photon index Γ). This is demonstrated through a 100 ks HEX-P simulation of a typical magnetar spectrum, i.e., $kT = 0.45$ keV, $\Gamma = 1.0$, and $N_{\rm H} = 10^{22}$ cm^{-2}, with absorption-corrected fluxes in the 1–10 keV and 10–100 keV band of 5.0×10^{-14} erg s^{-1} cm^{-2} and 10^{-13} erg s^{-1} cm^{-2}, respectively (Figure 2). The former flux level represents the faint end of the soft X-ray flux level from the currently known magnetar population while the latter is an order of magnitude fainter than the faintest magnetar hard X-ray tail known (SGR 0526–66; Park et al., 2020). The hard tail is detected up to 35 keV with a count rate of $(2.3 \pm 0.2) \times 10^{-3}$ counts s^{-1} (i.e., a 10σ detection significance), and the spectral curvature of the hard tail is constrained to 30% ($\Gamma = 1.0 \pm 0.3$). For comparison, we also perform a 100 ks simulated observation of the broad-band X-ray spectrum of the magnetar SGR 0526–66 in the Large Magellanic Cloud based on results from Chandra and NuSTAR (Park et al., 2020). HEX-P observations will produce a 10–80 keV count rate of $(44.3 \pm 0.2) \times 10^{-3}$ counts s^{-1} and a 0.5–10 keV rate of $(11.6 \pm 0.1) \times 10^{-2}$ counts s^{-1}, providing excellent quality data for a detailed spectral and temporal analysis. We note that, under the above spectral considerations, a simple 3.5σ detection of a fiducial magnetar at energies >10 keV with HET is achieved for fluxes as low as 4×10^{-14} erg s^{-1} cm^{-2}.

According to the current magnetar $\log N$-$\log S$ distribution (Figure 2, left panel), where S is the 10–100 keV flux, the HEX-P sensitivity limit will enable hard X-ray tail detection and characterization in about 30 magnetars, tripling the current number. Consequently, this will permit a far more comprehensive population-wide correlation analysis between the soft and hard X-ray properties (Marsden and White, 2001; Enoto et al., 2010; Kaspi and Boydstun, 2010; Enoto et al., 2017; Seo et al., 2023), in turn informing on the evolution of internal and external B-field and globally or locally twisted magnetospheres (Beloborodov, 2009; Parfrey et al., 2013; Viganò et al., 2013; Chen and Beloborodov, 2017).

Older magnetars, with spin-down ages $\gtrsim 10$ kyr, are less efficient at sustaining bright hard X-ray emission; their 1–100 keV luminosity is dominated by the soft thermal component from their surfaces (Enoto et al., 2010; Enoto et al., 2017). Hence, the LET is more suitable for the detection of older, fainter magnetars. We derive its detectability limit by considering a magnetar with a spectral model consisting of an absorbed ($N_{\rm H} = 10^{22}$ cm^{-2}) blackbody model with temperature $kT = 0.3$ keV (note that the magnetar surface temperature decreases with age, Viganò et al. 2013). We find that a 3.5σ detection can be achieved for observed fluxes of the order of 10^{-15} erg cm^{-2} s^{-1} (1–5 keV count rate of about $(5.5 \pm 1.5) \times 10^{-4}$ counts s^{-1}), rivaling the detection limit from XMM-Newton as well as Chandra. Hence, the LET provides an excellent opportunity to extend the legacy of the latter two observatories for the detection of the faint persistent counterparts to transient magnetars (Section 4.2).

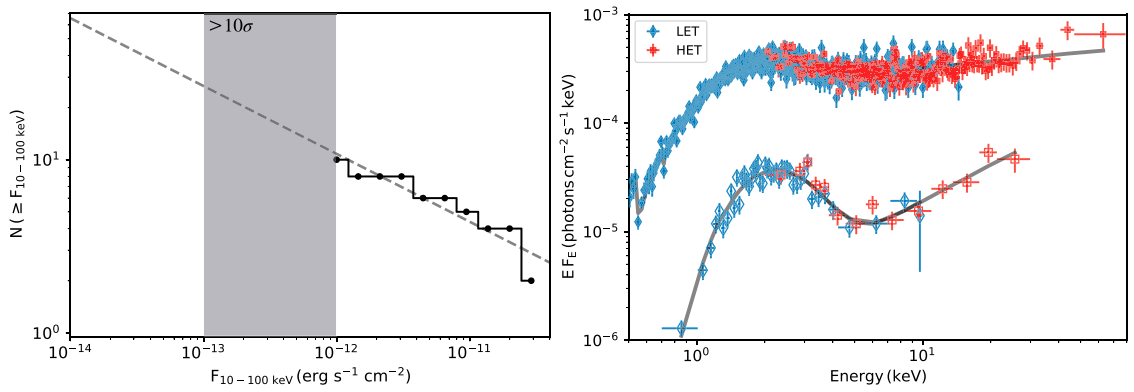

FIGURE 2
Left panel. Magnetar $\log N - \log S$ distribution in the hard (10–100 kev) X-ray band. NuSTAR doubled the number of magnetar detected at >10 keV, which currently stands at 10. The faintest hard X-ray tail known has a flux of the order 10^{-12} erg s^{-1} cm^{-2} (SGR 0526–66, Park et al., 2020. HEX-P, with its superior sensitivity, will triple the current number of hard X-ray tails detected from magnetars (gray shaded area). *Right panel.* 100 ks HEX-P simulation of the SGR 0526–66 broad-band spectrum (filled symbols) and of a generic magnetar with a hard X-ray flux in the 10–100 keV band an order of magnitude weaker than SGR 0526–66, i.e., $F_{10-100\ \rm keV} \sim 10^{-13}$ erg s^{-1} cm^{-2} (empty symbols).

For the brightest magnetars, HEX-P will also provide the most detailed look at the 0.3–80 keV spectro-temporal properties that are crucial to guide the theoretical development of radiation transport in the high B-field ($>10^{14}$ G) regime, inaccessible to terrestrial laboratories, such as photon splitting. Early predictions for the phase-resolved spectra and energy dependent profiles in the 10–80 keV band are presented in Wadiasingh et al. (2018), also see: Baring and Harding 2007; Fernández and Thompson 2007; Beloborodov 2013; Caiazzo et al., 2022; Taverna et al., 2020), and more sophisticated models are in development (e.g., Wadiasingh et al., 2019; Wadiasingh et al., 2022) Yet, the current data quality above 10 keV for even the brightest magnetars (i.e., 4U 0142 + 61 and 1RXS J170849.0−400,910), is inadequate for the detailed phase-resolved spectroscopy required to confront these models. HEX-P, providing far superior broad-band data for the brightest magnetars, will allow us to answer fundamental questions which currently remain open: 1) Where are the locales of particle acceleration within magnetar magnetospheres? 2) What are the Lorentz factors of the energetic particles? 3) How do the physical properties governing the hard X-ray tails evolve with age and field strength? 4) Is the hard X-ray emission for persistently emitting magnetars dominated by the dipolar field, or do higher order, crustal fields dominate?

RICS emission is highly anisotropic and sensitive to where cyclotron resonance in the magnetosphere is sampled by an observer. Moreover, beginning around 30 keV, photon splitting can begin to impact spectra depending in the viewing angle or, equivalently, pulse phase (Hu et al., 2019; Hu et al., 2022; Wadiasingh et al., 2022). As such, RICS radiation models may obtain a variety of phase-dependent spectral energy distributions (or equivalently, energy dependent pulse profiles) depending on viewing geometry and zones of activation of relativistic particle populations (Figure 3). Detailed fitting of phase-resolved spectra to models of RICS emission is sensitive to the activated zones and observer viewing geometry, providing answers to the open questions laid out above. Furthermore, a comparison of viewing and field geometries will test related constraints obtained for soft thermal emission hot spot modeling from IXPE observations of bright magnetars (Taverna et al., 2022; Zane et al., 2023).

RICS constraints on the relativistic electron population, along with 0.2–80 keV broadband spectroscopy provided by HEX-P will also test if return currents and particle bombardment play a significant role in heating surface layers of magnetars. Moreover, HEX-P will provide a detailed population-level phase-resolved spectral survey of magnetars. This will inform evolutionary traits in the RICS parameters with age, and determine if beaming is compatible with the lack of observed hard X-ray emission in some moderately bright X-ray magnetars. We note that fitting phase-resolved spectra with RICS models has not yet been attempted due to the paucity of pulsed counts at high energies (>10 keV). For instance, the brightest magnetar at hard X-rays, 1E 1841–045, has a *NuSTAR* count rate in the 10–79 keV band of 0.16 counts s^{-1}, which, for the 350 ks existing observation (An et al., 2015), results in 56,000 phase-averaged counts, and 11,200 pulsed counts. For a modest phase-resolved spectroscopic analysis with 10 phase bins, the 1100 counts in each bin were able to constrain the hard X-ray photon index to about ≈20% (An et al., 2015). In contrast, the HEX-P count rate for 1E 1841–045 in the same energy range is predicted to be 0.62 counts s^{-1}, which, for the same considerations above, would result in ~ 4350 counts per phase bin, allowing us to search for phase variability in the hard X-ray tail down to the $\lesssim 5$ percent level, notably aided by the LET instrument which will constrain the soft thermal part of the spectrum. Furthermore, observing from L1 rather than from low-Earth orbit like NuSTAR, HEX-P has nearly twice the observing efficiency of NuSTAR.

Lastly, we note that magnetars have attracted interest from the dark matter community as testbeds for certain axion-like particle (ALP) models. ALPs produced in the magnetar core are predicted to convert into photons in the magnetosphere. ALP models generally predict an opposite hard X-ray phase dependence to RICS, thereby enabling HEX-P to provide important constraints to the dark matter community (e.g., Maruyama et al., 2018; Fortin et al., 2021).

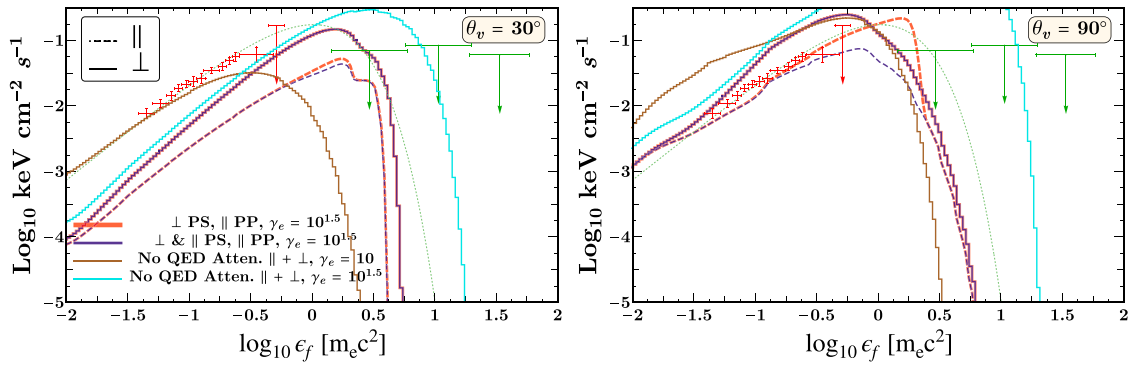

FIGURE 3
Phase-resolved RICS spectra overlaid on INTEGRAL data for 4U 0142 + 61 (orange data points, Kuiper et al., 2006), along with a power-law with exponential cutoff at 350 keV (dotted green). The model emission is computed for surface photons of temperature 5×10^6 K scattered by $\gamma_e = 10$-$10^{1.5}$ electrons uniformly populating field bundle from magnetic footpoint colatitudes 12°–45°. The assumed dipole field strength is 4×10^{14} G. Brown and dark blue lines show total intensities, while red and light blue curves show the case with QED attenuation. *Left panel.* Observer angle to magnetic axis $\theta_v = 30°$. *Right panel.* $\theta_v = 90°$. The RICS emission is predicted to be highly phase dependent, as shown here. Adapted from Wadiasingh et al. (2019).

4.2 Transient behavior–crustal and magnetospheric dynamics

In addition to the persistent magnetars, with X-ray luminosities $\sim 10^{35}$ erg s^{-1}, there are also 'transient' magnetars, which only reach $\sim 10^{35}$ erg s^{-1} during outbursts, when their X-ray fluxes can increase by up to over two orders of magnitude (Coti Zelati et al., 2018). We emsphasize that persistent magnetars also experience outbursts, with the distinction between 'persistent' and 'transient' magnetar dependent on the initial quiescent luminosity of each source Pons and Rea (2012). Transient magnetar outbursts decay on exponential timescales ranging from months to years (Rea et al., 2009; Kaspi et al., 2014; Coti Zelati et al., 2018). The outburst spectra feature both thermal emission and transient non-thermal emission. The non-thermal emission is observed only during outbursts, and is believed to have a magnetospheric origin. The thermal emission is observed both during quiescence and outburst, is brighter and harder during outbursts, and is thought to originate from the NS surface.

During the decay phase, thermal hot spots are observed to cool and shrink in size. This behaviour is consistent with currents circulating through a twisted magnetosphere, depositing heat at the surface footpoints of magnetic current loops Beloborodov (2009). Alternatively, this behavior might be due to internal heating of the crust through magnetic stresses associated with evolving toroidal fields (Lander et al., 2015; Lander and Gourgouliatos, 2019; Lander, 2023). While the decay of the thermal emission has been well observationally constrained, the hard, non-thermal X-ray emission fades beyond current detection limits fairly quickly (over the course of weeks). It is therefore unknown whether the non-thermal emission decays in tandem with the soft X-ray emission, as expected in the case of surface bombardment by accelerated particles in the magnetosphere, or whether the two evolve independently. This might be the case if the surface heating is indeed induced internally (e.g., Kouveliotou et al., 2004; Pons and Rea, 2012; Deibel et al., 2017), independent of the external magnetospheric emission. This is a major open question in transient magnetars given its potential to investigate crustal micro- and macro-physical properties, which are poorly known, and are highly relevant to the NS equation of state. HEX-P's sensitivity and broadband X-ray coverage are uniquely capable of addressing this fundamental open question.

The left panel of Figure 4 shows simulated HEX-P and NuSTAR spectra, both with 100 ks exposure time, based on the X-ray spectrum of the transient magnetar XTE J1810-197 during its late 2018 outburst (Gotthelf et al., 2019). These simulations highlight the essential role that the LET plays in constraining the soft <2 keV spectrum, especially in the case of less absorbed sources such as for XTE J1810-197, and the ~5x increase in counts for the HET vs. NuSTAR.

The right panel of Figure 4 shows HEX-P and NuSTAR simulations, both with 100 ks exposure time, of the hard X-ray spectrum of SGR J1745−2900 following its 2013 outburst. The spectral parameters are set based on NuSTAR and Chandra observations of the beginning of the 2013 outburst (Kaspi et al., 2014). The hard non-thermal emission could only be tracked for ~4 months post-outburst, due to the crowded nature of the galactic center (GC) region. On the other hand, we know that the soft thermal emission temperature and luminosity followed a multi-year evolution observed by Chandra (Figure 5, left panel) (Rea et al., 2020). Since Chandra's excellent angular resolution enabled multi-year tracking of the soft emission, it is natural so to ask how long HEX-P can track the evolution of the hard X-ray emission. We emphasize that such observation are only possible due to HEX-P's *combined* excellent angular resolution (important in the GC region) and larger effective area than NuSTAR. We perform our simulations by setting the luminosity of the non-thermal emission equal to what was observed by NuSTAR at the beginning of the outburst, and set the non-thermal emission to decay proportionally to the thermal luminosity. All observations are simulated with a 100 ks exposure time. While NuSTAR tracked the SGR J1745−2900 non-thermal emission for only 4 months post-outburst, we calculate that HEX-P will be capable of tracking a similar magnetar outburst for 2 years (Figure 5, right panel). While the biggest advantage of HEX-P in this scenario (vs. previous observatories, e.g., Chandra)

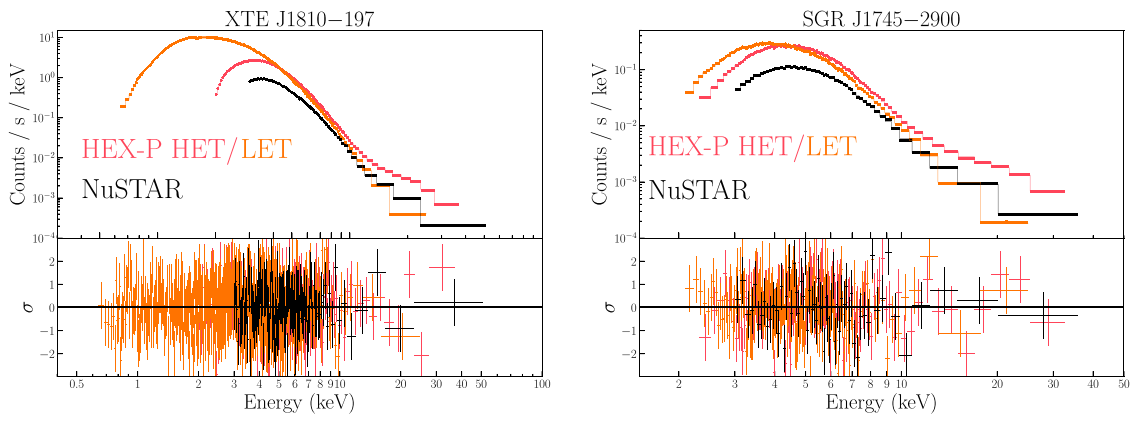

FIGURE 4
Simulated HEX-P broadband X-ray spectra of two transient magnetars near the peak of their outbursts: XTE J1810–197 (left) and SGR J1745–2900 (right) based on data from their 2018 and 2013 outbursts, respectively. LET and HET data are shown in orange and red, respectively. Note that SGR J1745–2900 is highly absorbed due to its location in the Galactic center region.

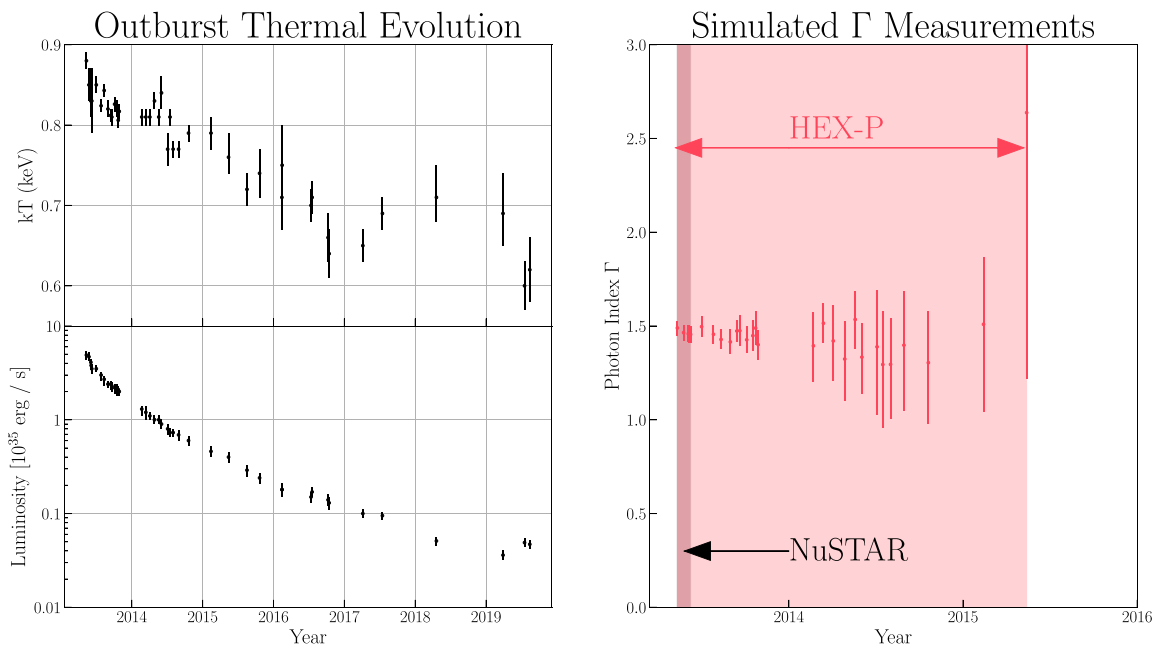

FIGURE 5
Simulated HEX-P measurements of the photon index Γ following the 2013 outburst of SGR 1745–2900 based on NuSTAR and Chandra observations. The upper panel of the left figure shows the evolution of the blackbody temperature, where the evolution of the 0.3–10.0 keV X-ray luminosity is shown in the lower panel of the left figure. The right figure shows the evolution of Γ obtained with NuSTAR and HEX-P. HEX-P's improved sensitivity will enable monitoring of these outbursts significantly longer than NuSTAR.

is its ability to track the hard X-ray decay, we also mention that its broadband coverage will also allow for more precise measurements of the soft thermal emission temperature and flux. This will provide data critical to our understanding of NS crustal and magnetospheric dynamics, unique observational characteristics of magnetars following an outburst.

4.3 Fast radio bursts

Fast Radio Bursts (FRBs) are millisecond, bright radio bursts (fluence ~ few Jy ms) observed over a broad range of frequencies, from ~120 MHz to a few GHz. They were first reported in 2007 (Lorimer et al., 2007), and since then several hundred have been detected by a suite of radio dishes across the Earth, e.g., Parkes, Arecibo, ASKAP, FAST, and CHIME (Petroff et al., 2022). FRBs are distributed nearly isotropically across the sky and show very large dispersion measures, indicating an extragalactic origin. Hence, their large fluences translate into very bright luminosities, ~9 orders of magnitude brighter than the Crab's giant pulses. While most FRBs appear as single events, a few have associated with a single position on the sky, i.e., repeating FRBs (Fonseca et al., 2020). The origin of FRBs is currently a matter of intense debate, and while many theoretical possibilities exist (Platts et al., 2019), one of the leading models is a NS or magnetar central engine.

In a breakthrough discovery, observational evidence for the magnetar model as a source of FRBs occurred on 2020 April 28, when an FRB-like radio burst was detected from the Galactic magnetar SGR 1935 + 2154 (CHIME/FRB Collaboration et al., 2020; Bochenek et al., 2020), in the winding hours of a major burst storm (Younes et al., 2020); it had a fluence rivaling those of the faint end of extragalactic FRBs. Moreover, the FRB occurred simultaneously with a bright, short X-ray burst, connecting it to magnetar activity and providing crucial evidence for its triggering mechanism (e.g., Mereghetti et al., 2020; Li et al., 2021; Ridnaia et al., 2021). In the following years, SGR 1935 + 2154 has shown several more radio bursts (Kirsten et al., 2020), most notably at times of bursting activity. Though most radio bursts occur simultaneous to X-ray bursts, the majority of X-ray bursts occur without a simultaneous radio signal (Lin et al., 2020b; Bailes et al., 2021) suggesting special circumstances for the emission of FRB-like bursts from magnetars. Indeed, a comparison of the X-ray burst associated with the FRB and NICER + Fermi bursts belonging to the same burst storm of April 2020 reveal the former to have a distinctive spectrum. This is a clue to either its emission mechanism or triggering locale (Younes et al., 2021), and has been seen in data from INTEGRAL (Mereghetti et al., 2020), Fermi/GBM (Lin et al., 2020a), Konus-Wind (Ridnaia et al., 2021), and Insight-HXMT (Li et al., 2021), among others.

The discovery of FRB-like bursts from magnetars opened up new avenues for the study of extragalactic FRBs (e.g., Wadiasingh and Timokhin, 2019), radio emission from young INSs (Philippov and Kramer, 2022), and, more generally, plasma and pair production in magnetar magnetospheres (e.g., Beloborodov, 2020; Yuan et al., 2020; Mahlmann et al., 2022). Yet, as is the case with every new fundamental discovery, more questions arise in its aftermath, e.g., 1) What is unique about the FRB-associated X-ray bursts, and why do the majority of X-ray bursts lack a radio counterpart? (2) What

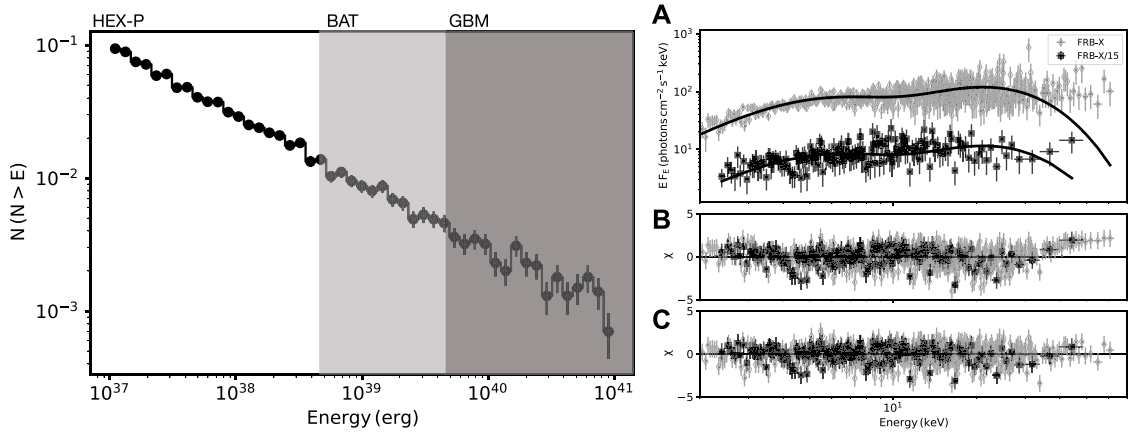

FIGURE 6
Left panel. $\log N - \log E$ distribution of magnetar short bursts, where E is the burst total energy. The light and dark shaded areas are the sensitivity limits (>5σ detection) of Swift/BAT and Fermi/GBM, respectively, assuming a source distance of 20 kpc. HEX-P is sensitive to the full burst energy distribution for every magnetar in the Galaxy. *Right panel.* Panel **(A)** shows a HEX-P Xspec simulation of the FRB200428-associated X-ray burst spectrum (gray diamonds) assuming a non-thermal cutoff power-law as measured with Insight-HXMT (Li et al., 2021). The solid line is the best-fit thermal double blackbody (2BB) model. Black squares are a simulated spectrum with the same assumptions, but with a fluence that is a factor 15 smaller. Panel **(B)** shows the residuals from the thermal fit in units of 1σ, with the same grey and black symbols. Panel **(C)** shows the residuals from the non-thermal fit in units of 1σ, again with the same grey and black symbols. HEX-P will distinguish the thermal vs. non-thermal nature of short X-ray bursts for fluences that are over an order of magnitude weaker than FRB-X (see text).

is the distribution of the spectral properties for FRB-associated X-ray bursts? Are their distinctive spectral properties universal across radio fluence? 3) Is the radio to X-ray flux ratio (L_R/L_X) constant for all FRB-like radio bursts? 4) What is the radio-X-ray time-lag across burst fluence?

The answers to these open questions are critical for improving our understanding of the FRB phenomenon, both Galactic and extragalactic. Answering these questions will require 1) a broad X-ray coverage given that the spectral energy distributions of magnetar bursts peak in the 20–30 keV range, 2) high timing resolution ($\lesssim$ 1 ms) for accurately measuring the radio-X-ray lag in burst arrival time (Mereghetti et al., 2020), 3) sensitivity to faint X-ray bursts, i.e., fluence $<10^{-7}$ erg cm^{-2}, to sample a large fraction of the X-ray and radio burst fluence distribution given their steep shapes ($N \propto S^{-0.6}$, Figure 6; Younes et al., 2020). HEX-P is the only facility to satisfy all the above criteria. Its only limitation is the small field-of-view, yet, most radio FRB bursts detected from the Galactic magnetar SGR 1935 + 2154 occurred at the time of major burst storms, which last up to a few days. This is sufficient time for HEX-P to slew to the target. We also note that NuSTAR was observing SGR 1935 + 2154 at the time of its 2022 October FRB-like burst, though the source was Earth-occulted (Dong and Chime/Frb Collaboration, 2022; Enoto et al., 2022). Due to the L1 orbit of HEX-P, such misfortune is naturally avoided.

The left panel of Figure 6 shows a simulated $\log N - \log S$ magnetar burst energy distribution, which follows a power-law of the form $dN/dE \propto E^{-1.6}$ (GöğüŞ et al., 1999; Göğüş et al., 2000; Gavriil et al., 2004; van der Horst et al., 2012; Younes et al., 2020). The Fermi/GBM >5σ sensitivity to typical short bursts from a magnetar at a distance of 20 kpc is shown in dark gray (Meegan et al., 2009) while that for Swift/BAT is shown in light gray (Lien et al., 2016). At that distance, HEX-P will detect bursts with energies comparable to the persistent emission, i.e., ~10^{37} erg (in a 1-s interval), covering significantly more of the short burst energy distribution. This will ensure the detection of X-ray bursts associated with faint radio bursts and provide answers to questions (3) and (4).

To address questions (1) and (2), we performed HEX-P HET simulations of an X-ray burst with spectral properties similar to that of the FRB-associated X-ray burst (which we call FRB-X) as determined by Insight-HXMT (Li et al., 2021); i.e., a cutoff power-law with $\Gamma = 1.6$ and $E_{cut} = 80$ keV, and a fluence of 5.0×10^{-7} erg cm^{-2} (Figure 6, gray diamonds in panel (a)), and a burst-duration of 1 s. We then fit this spectrum with a thermal 2 blackbody (2BB) model (shown as a solid black line). The thermal model fails to provide a statistically acceptable fit to the data (panel (b)), unlike the non-thermal model (panel (c)). This is confirmed through Xspec simulations which show that $\gg$ 99% of simulated spectra drawn from the thermal model have better fit statistics. This indicates that Het alone will discern the non-thermal nature of any bursts similar to FRB-X. We then performed a set of simulations assuming the same spectral model as FRB-X, while decreasing the fluence by increments of factor 2. We then fit each spectrum to a thermal 2BB model, and assess the fit quality through simulations. We find that we can discern (at the ≈3σ level) between the thermal and non-thermal model down to a fluence of ~3×10^{-8} erg cm^{-2}, i.e., a factor 15 fainter than FRB-X (Figure 6, black squares).

5 Central compact objects

The CCO class of NSs are defined by the following observational characteristics: steady, soft thermal X-ray emission, lack of a surrounding pulsar wind nebula, and non-detection at all other wavelengths. X-ray pulses have been detected from only three of the dozen known CCOs (Gotthelf et al., 2013). Two of these three, the CCOs in the Puppis A and Kes 79 SNRs, have the lowest spin

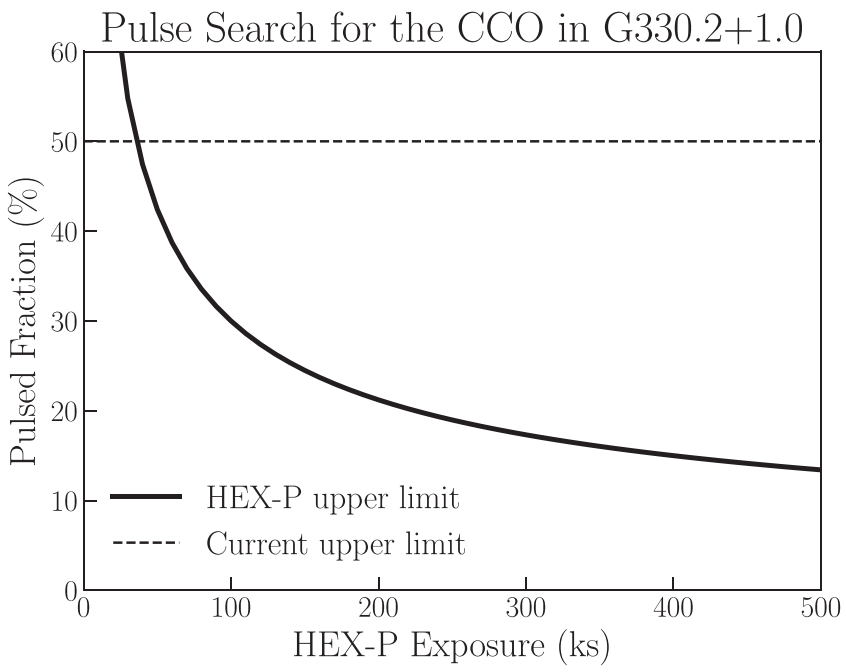

FIGURE 7
HEX-P pulsed fraction upper limits as a function of exposure for the CCO in G330.2 + 1.0.

down measured magnetic fields among young neutron stars, with $B_s \sim 3 \times 10^{10}$ G.

While only a dozen CCOs are currently known, their locations in young SNRs indicates they may represent a significant fraction of all NS births. Hence, understanding how young NSs are born with such small dipole magnetic fields is important to address how CCOs fit within the broad INS family. Increasing the number of CCO spin period and period derivative measurements is critical. Because CCOs are only detected at X-ray wavelengths, these spin period searches can only be done in the X-ray band. This is an area where HEX-P can shine as a follow-up observatory, capable of both searching for X-ray pulsations and, after identifying a spin period, making the required phase resolved spectroscopic measurements.

As an example, the CCO in G330.2 + 1.0 is a promising target for HEX-P thermal pulse searches. Previous searches with XMM-Newton were limited by the high background from the surrounding SNR thermal emission (Alford and Halpern, 2023). This is highlighted in Eq. 1 which relates the calculated pulsed fraction upper limit $f_p^{\max}$ to the number of total counts N, source counts N_s, background counts N_b, and intrinsic signal power P_s:

$$f_p^{\max} = 2\left(1 + N_b/N_s\right)\sqrt{P_s/N}, \quad (1)$$

Since CCOs are found in young supernova remnants, in many cases the thermal background emission from the remnant can be significant, hindering the ability to detect the underlying NS pulsations. To overcome these obstacles, both high X-ray timing and angular resolution are required. HEX-P's 3.5 arcsec PSF (for the LET detector) will allow for a significantly reduced background. Detailed comparisons of the performance of HEX-P in pulsar searches compared to XMM-Newton and NuSTAR can be found in Bachetti et al., in prep. (ULXs and extragalactic pulsars) and Mori et al., in prep. (the Galactic Center). Figure 7 presents the pulsed fraction upper limits as a function of exposure time for the CCO in G330.2 + 1.0. HEX-P will significantly reduce the current pulsed fraction upper limit, likely leading to a secure determination of the spin period.

Once an X-ray pulse period is found, a measurement of the period derivative can easily follow, as well as the characterization of the timing properties of these sources, e.g., B-field strength and spin down luminosity $\dot{E}$. Moreover, such observations will allow us to study the thermal pulse profiles of new CCOs. Energy-dependent pulse profile modeling is a powerful tool to map the surface thermal emission (Bogdanov, 2014; Alford et al., 2022). The HEX-P LET has the required effective area, timing resolution, low background, and angular resolution to produce more detailed maps, while increasing the pool of studied sources.

6 Rotation-powered pulsars

In contrast to the magnetically-powered magnetars and passively cooling CCOs, many pulsars are powered by the loss of their rotational kinetic energy. The 33 ms Crab pulsar is perhaps the best known pulsar in this class, with significant rotationally powered emission extending into the hard X-ray band (Madsen et al., 2015). HEX-P observations of the Crab pulsar will be a significant improvement over NuSTAR. For instance, HEX-P will enable low background phase-resolved studies of the Crab pulsar, by resolving the Crab pulsar from the bright pulsar wind nebula (PWN) background emission.

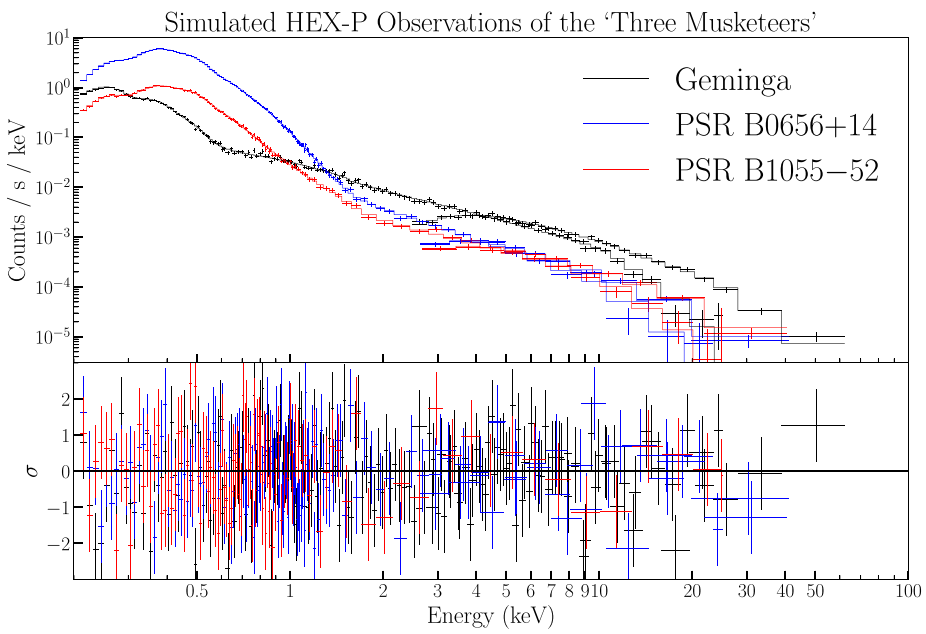

FIGURE 8
Simulated HEX-P observations of the Geminga pulsar, PSR B0656 + 14, and PSR B1055-52. HEX-P will be capable of extending the current hard X-ray detection limit for Geminga from 20 keV to 50 keV.

HEX-P will allow us to observe in detail the faint, middle-aged (~10^5 yr) pulsars which offer an opportunity to study how pulsars evolve and eventually "die," ceasing as X-ray and radio emitting sources. As RPPs age, their X-ray luminosity will decrease with their spin down power, making observations more challenging compared to younger RPPs.

There are three well-known nearby middle-aged pulsars that have been dubbed the "three musketeers": PSR B0656 + 14, PSR B1055−52 and Geminga. These three pulsars all exhibit thermal surface emission and non-thermal magnetospheric emission. They have similar ~10^{12} G spin down magnetic fields and 10^{34} erg s^{-1} spin down luminosities (De Luca et al., 2005). Despite their relative proximity, open questions remain regarding the physics of their surface thermal emission, and the extent of their non-thermal emission.

Open questions about Geminga are particularly interesting given its potentially large contribution to the local leptonic cosmic ray flux, and its status as the second brightest gamma-ray source in the sky. Mori et al. (2014) reported on a 150 ks NuSTAR observation of Geminga and found several spectral models were consistent with the data. Figure 8 shows a simulated 200 ks HEX-P observation of Geminga based on the two blackbody plus powerlaw model, with $\Gamma = 1.7$, $kT_1 = 44$ eV, and $kT_2 = 195$ eV. The cooler thermal component corresponds to emission from the whole NS surface, and the hot component, if its existence is confirmed, may correspond to emission from a hot polar cap. We find that, if the powerlaw extends to higher energies, HEX-P will extend the detection of non-thermal emission from ~20 keV to ~50 keV. The X-ray emission of Geminga above 20 keV is unexplored territory, and the detection of changes in the spectrum could be important clues to the physics of its magnetosphere.

Figure 8 also shows simulated HEX-P observations of PSR B0656 + 14 and PSR B1055−52, performed using the spectral parameters from De Luca et al. (2005). We find that 150 ks HEX-P observations will measure the photon indices Γ of all three of these faint pulsars to better than 10%.

HEX-P will also potentially address a fundamental mystery regarding PSR B0656 + 14, PSR B1055−52 and Geminga. B0656 + 14, and PSR B1055−52 clearly have small surface thermal hot spots, presumably corresponding to the heated pulsar polar caps. If Geminga has a similar hot spot, then its luminosity is at least two orders of magnitude dimmer (Jackson and Halpern, 2005). HEX-P's high throughput and broad coverage of Geminga's X-ray spectrum will allow us to answer this question.

7 Potential discovery space

Present and future large field-of-view facilities at all wavelengths from radio to PeV energies will result in a large number of unidentified sources, especially within the Galactic plane. This is already evident at GeV energies and beyond, i.e., Fermi/LAT, H.E.S.S, and LHASSO, where the number of unknown sources outweigh the number of identified ones, a problem that will only be exacerbated with the Cherenkov Telescope Array Observatory (CTAO). These high energy sources represent the most efficient particle accelerators in the universe, and for the Galactic ones, their most likely counterpart involves a pulsar (Mori et al., 2014 (in prep.)). At X-ray energies, eROSITA (Predehl et al., 2021, and potentially STAR-X Zhang et al., 2022) will provide some of the deepest wide-field X-ray surveys of our Galaxy, with a >10× increase in the number of X-ray sources compared to ROSAT. A large

fraction of these X-ray sources will be of unknown origin, and a non-negligible fraction should be INSs (Pires et al., 2017). Deeper, targeted exposures, as possible with HEX-P, will be required to identify them. Finally, in the radio, the Square Kilometer Array and Deep Synoptic Array 2000 are expected to increase the number of currently known pulsars by a factor of 10 (i.e., to ~20,000 pulsars), as well as detect a large number of new SNR shells and candidate wind nebulae.

Simply detecting X-ray point sources in the error region of unidentified gamma-ray and radio sources will not yield a secure identification. Furthermore, providing a high quality soft X-ray spectrum of eROSITA/STAR-X sources will not be enough to firmly distinguish their origin. High timing resolution is required to discern the pulsar nature from other types of X-ray emitters, such as low-mass X-ray binaries, cataclysmic variables, background active galaxies, etc. Moreover, being limited to a soft X-ray detector will hamper our ability to probe deep into the Galaxy due to absorption, stressing the need for hard X-ray coverage. Last but not least, high spatial resolution is required for crowded regions such as Sgr A* (Mori et al., 2014 (in prep.)), and to isolate the pulsar emission from any surrounding SNR and/or nebula (as noted in §5 with regards to candidate CCOs). These issues have already been demonstrated with NuSTAR. For instance, although a candidate soft X-ray counterpart to the TeV γ-ray source HESS J1640-465 had been proposed, only NuSTAR was able to detect pulsed emission confirming its pulsar nature (Gotthelf et al., 2019). This was mainly due to the combination of heavy absorption (10^{23} cm^{-2}) in the source direction and non-negligible contamination by the PWN (Gotthelf et al., 2019). Continued NuSTAR follow-up of this pulsar found the braking index $n > 3$, possibly pointing to a magnetic quadrupole in the source (Archibald et al., 2016a).

HEX-P presents the ideal satellite to follow-up Galactic gamma-ray sources, INS candidates from wide-area X-ray surveys, and pulsar/pulsar candidates from deep radio surveys. Increasing the number of isolated X-ray pulsars, such as XDINs, CCOs, RPPs, and magnetars, will enable a deeper understanding of their physics, X-ray properties, environment (e.g., wind nebulae, SNRs and nearby cosmic ray acceleration sites), and progenitors, in turn teaching us about NS formation and evolutionary tracks through, e.g., population synthesis modeling (e.g., Gullón et al., 2015; Dirson et al., 2022) and magneto-thermal evolution models (e.g., Viganò et al., 2013; Gourgouliatos et al., 2016).

Data availability statement

The original contributions presented in the study are included in the article/Supplementary Material, further inquiries can be directed to the corresponding author.

Author contributions

JA: Conceptualization, Investigation, Software, Writing–original draft, Writing–review and editing. GY: Writing–original draft, Writing–review and editing. ZW: Writing–review and editing, Writing–original draft. MA: Writing–review and editing. HA: Writing–review and editing. MBc: Writing–review and editing. MBr: Writing–review and editing. AB: Writing–review and editing. AC: Writing–review and editing. TE: Writing–review and editing. JAG: Writing–review and editing. JDG: Writing–review and editing. EG: Writing–review and editing. AH: Writing–review and editing. C-PH: Writing–review and editing. AJ: Writing–review and editing. VK: Writing–review and editing. CKi: Writing–review and editing. CKo: Writing–review and editing. LK: Writing–review and editing. KM: Writing–review and editing. MN: Writing–review and editing. JP: Writing–review and editing. DS: Writing–review and editing. JV: Writing–review and editing. DW: Writing–review and editing.

Funding

The author(s) declare financial support was received for the research, authorship, and/or publication of this article. The work of DS was carried out at the Jet Propulsion Laboratory, California Institute of Technology, under a contract with NASA. ZW acknowledges support by NASA under award number 80GSFC21M0002. This work has made use of the NASA Astrophysics Data System.

Conflict of interest

The authors declare that the research was conducted in the absence of any commercial or financial relationships that could be construed as a potential conflict of interest.

The reviewer AB declared a past co-authorship with the author GY to the handling editor.

Publisher's note

References

Alford, J. A. J., Gotthelf, E. V., Perna, R., and Halpern, J. P. (2022). Measuring the nonaxially symmetric surface temperature distribution of the central compact object in Puppis A. *ApJ* 927, 233. doi:10.3847/1538-4357/ac4d9a

Alford, J. A. J., and Halpern, J. P. (2023). Do central compact objects have carbon atmospheres? *ApJ* 944, 36. doi:10.3847/1538-4357/acaf55

An, H., Archibald, R. F., Hascoët, R., Kaspi, V. M., Beloborodov, A. M., Archibald, A. M., et al. (2015). Deep NuSTAR and Swift monitoring observations of the magnetar 1E 1841-045. *ApJ* 807, 93. doi:10.1088/0004-637X/807/1/93

Archibald, R. F., Gotthelf, E. V., Ferdman, R. D., Kaspi, V. M., Guillot, S., Harrison, F. A., et al. (2016a). A high braking index for a pulsar. *ApJL* 819, L16. doi:10.3847/2041-8205/819/1/L16

Archibald, R. F., Kaspi, V. M., Tendulkar, S. P., and Scholz, P. (2016b). A magnetar-like outburst from a high-B radio pulsar. *ApJL* 829, L21. doi:10.3847/2041-8205/829/1/L21

Arnaud, K. A. (1996). "XSPEC: the first ten years," in *Astronomical data analysis software and systems V of astronomical society of the pacific conference series*. Editors G. H. Jacoby, and J. Barnes 101, 17.

Arzoumanian, Z., Chernoff, D. F., and Cordes, J. M. (2002). The velocity distribution of isolated radio pulsars. *ApJ* 568, 289–301. doi:10.1086/338805

Bailes, M., Bassa, C. G., Bernardi, G., Buchner, S., Burgay, M., Caleb, M., et al. (2021). Multifrequency observations of SGR J1935+2154. *MNRAS* 503, 5367–5384. doi:10.1093/mnras/stab749

Baring, M. G., and Harding, A. K. (2007). Resonant Compton upscattering in anomalous X-ray pulsars. *APSS* 308, 109–118. doi:10.1007/s10509-007-9326-x

Beloborodov, A. M. (2009). Untwisting magnetospheres of neutron stars. *ApJ* 703, 1044–1060. doi:10.1088/0004-637X/703/1/1044

Beloborodov, A. M. (2013). On the mechanism of hard X-ray emission from magnetars. *ApJ* 762, 13. doi:10.1088/0004-637X/762/1/13

Beloborodov, A. M. (2020). Blast waves from magnetar flares and fast radio bursts. *ApJ* 896, 142. doi:10.3847/1538-4357/ab83eb

Beniamini, P., Wadiasingh, Z., Hare, J., Rajwade, K. M., Younes, G., and van der Horst, A. J. (2023). Evidence for an abundant old population of Galactic ultra-long period magnetars and implications for fast radio bursts. *MNRAS* 520, 1872–1894. doi:10.1093/mnras/stad208

Bochenek, C. D., Ravi, V., Belov, K. V., Hallinan, G., Kocz, J., Kulkarni, S. R., et al. (2020). A fast radio burst associated with a Galactic magnetar. *Nature* 587, 59–62. doi:10.1038/s41586-020-2872-x

Bogdanov, S. (2014). Modeling the X-rays from the central compact object PSR J1852+0040 in kesteven 79: evidence for a strongly magnetized neutron star. *ApJ* 790, 94. doi:10.1088/0004-637X/790/2/94

Caiazzo, I., González-Caniulef, D., Heyl, J., and Fernández, R. (2022). Probing magnetar emission mechanisms with X-ray spectropolarimetry. *MNRAS* 514, 5024–5034. doi:10.1093/mnras/stac1571

Caleb, M., Heywood, I., Rajwade, K., Malenta, M., Stappers, B. W., Barr, E., et al. (2022). Discovery of a radio-emitting neutron star with an ultra-long spin period of 76 s. *Nat. Astron.* 6, 828–836. doi:10.1038/s41550-022-01688-x

Camilo, F., Ransom, S. M., Halpern, J. P., and Reynolds, J. (2007). 1E 1547.0-5408: a radio-emitting magnetar with a rotation period of 2 seconds. *ApJL* 666, L93–L96. doi:10.1086/521826

Camilo, F., Ransom, S. M., Halpern, J. P., Reynolds, J., Helfand, D. J., Zimmerman, N., et al. (2006). Transient pulsed radio emission from a magnetar. *Nature* 442, 892–895. doi:10.1038/nature04986

Cash, W. (1979). Parameter estimation in astronomy through application of the likelihood ratio. *ApJ* 228, 939–947. doi:10.1086/156922

Chen, A. Y., and Beloborodov, A. M. (2017). Particle-in-Cell simulations of the twisted magnetospheres of magnetars. I. *ApJ* 844, 133. doi:10.3847/1538-4357/aa7a57

CHIME/FRB Collaboration, Andersen, B. C., Bandura, K. M., Bhardwaj, M., Bij, A., Boyce, M. M., et al. (2020). A bright millisecond-duration radio burst from a Galactic magnetar. *Nature* 587, 54–58. doi:10.1038/s41586-020-2863-y

Coti Zelati, F., Rea, N., Pons, J. A., Campana, S., and Esposito, P. (2018). Systematic study of magnetar outbursts. *MNRAS* 474, 961–1017. doi:10.1093/mnras/stx2679

Deibel, A., Cumming, A., Brown, E. F., and Reddy, S. (2017). Late-time cooling of neutron star transients and the physics of the inner crust. *ApJ* 839, 95. doi:10.3847/1538-4357/aa6a19

De Luca, A. (2017). Central compact objects in supernova remnants. *J. Phys. Conf. Ser. J. Phys. Conf. Ser.* 932, 012006. doi:10.1088/1742-6596/932/1/012006

De Luca, A., Caraveo, P. A., Mereghetti, S., Negroni, M., and Bignami, G. F. (2005). On the polar caps of the three musketeers. *ApJ* 623, 1051–1069. doi:10.1086/428567

den Hartog, P. R., Kuiper, L., and Hermsen, W. (2008a). Detailed high-energy characteristics of AXP 1RXS J170849-400910. Probing the magnetosphere using INTEGRAL, RXTE, and XMM-Newton. *A&A* 489, 263–279. doi:10.1051/0004-6361:200809772

den Hartog, P. R., Kuiper, L., Hermsen, W., Kaspi, V. M., Dib, R., Knödlseder, J., et al. (2008b). Detailed high-energy characteristics of AXP 4U 0142+61. Multi-year observations with INTEGRAL, RXTE, XMM-Newton, and ASCA. *A&A* 489, 245–261. doi:10.1051/0004-6361:200809390

Dirson, L., Pétri, J., and Mitra, D. (2022). The Galactic population of canonical pulsars. *A&A* 667, A82. doi:10.1051/0004-6361/202243305

Dong, F. A., and Chime/Frb Collaboration (2022). *CHIME/FRB detection of a bright radio burst from SGR 1935+2154*. The Astronomer's Telegram, 15681.

Enoto, T., Hu, C.-P., Guver, T., Younes, G., Gendreau, K. C., Arzoumanian, Z., et al. (2022). *NICER and NuSTAR observations of SGR 1935+2154 bracketing the time of the bright radio burst*. The Astronomer's Telegram, 15690.

Enoto, T., Nakazawa, K., Makishima, K., Rea, N., Hurley, K., and Shibata, S. (2010). Broadband study with suzaku of the magnetar class. *ApJL* 722, L162–L167. doi:10.1088/2041-8205/722/2/L162

Enoto, T., Shibata, S., Kitaguchi, T., Suwa, Y., Uchide, T., Nishioka, H., et al. (2017). Magnetar broadband X-ray spectra correlated with magnetic fields: suzaku archive of SGRs and AXPs combined with NuSTAR, Swift, and RXTE. *ApJS* 231, 8. doi:10.3847/1538-4365/aa6f0a

Eraerds, T., Antonelli, V., Davis, C., Hall, D., Hetherington, O., Holland, A., et al. (2021). Enhanced simulations on the athena/wide field imager instrumental background. *J. Astronomical Telesc. Instrum. Syst.* 7, 034001. doi:10.1117/1.JATIS.7.3.034001

Faucher-Giguère, C.-A., and Kaspi, V. M. (2006). Birth and evolution of isolated radio pulsars. *ApJ* 643, 332–355. doi:10.1086/501516

Fernández, R., and Thompson, C. (2007). Resonant cyclotron scattering in three dimensions and the quiescent nonthermal X-ray emission of magnetars. *ApJ* 660, 615–640. doi:10.1086/511810

Fonseca, E., Andersen, B. C., Bhardwaj, M., Chawla, P., Good, D. C., Josephy, A., et al. (2020). Nine new repeating fast radio burst sources from CHIME/FRB. *ApJL* 891, L6. doi:10.3847/2041-8213/ab7208

Fortin, J.-F., Guo, H.-K., Harris, S. P., Sheridan, E., and Sinha, K. (2021). Magnetars and axion-like particles: probes with the hard X-ray spectrum. *JCAP* 2021, 036. doi:10.1088/1475-7516/2021/06/036

Gavriil, F. P., Gonzalez, M. E., Gotthelf, E. V., Kaspi, V. M., Livingstone, M. A., and Woods, P. M. (2008). Magnetar-like emission from the young pulsar in kes 75. *Science* 319, 1802–1805. doi:10.1126/science.1153465

Gavriil, F. P., Kaspi, V. M., and Woods, P. M. (2004). A comprehensive study of the X-ray bursts from the magnetar candidate 1E 2259+586. *ApJ* 607, 959–969. doi:10.1086/383564

Göğüş, E., Woods, P. M., Kouveliotou, C., van Paradijs, J., Briggs, M. S., Duncan, R. C., et al. (2000). Statistical properties of SGR 1806-20 bursts. *ApJL* 532, L121–L124. doi:10.1086/312583

GöğüŞ, E., Woods, P. M., Kouveliotou, C., van Paradijs, J., Briggs, M. S., Duncan, R. C., et al. (1999). Statistical properties of SGR 1900+14 bursts. *ApJL* 526, L93–L96. doi:10.1086/312380

Gotthelf, E. V., Halpern, J. P., and Alford, J. (2013). The spin-down of PSR j0821-4300 and PSR j1210-5226: confirmation of central compact objects as anti-magnetars. *ApJ* 765, 58. doi:10.1088/0004-637X/765/1/58

Gotthelf, E. V., Halpern, J. P., Alford, J. A. J., Mihara, T., Negoro, H., Kawai, N., et al. (2019). The 2018 X-ray and radio outburst of magnetar XTE j1810-197. *ApJL* 874, L25. doi:10.3847/2041-8213/ab101a

Gourgouliatos, K. N., Wood, T. S., and Hollerbach, R. (2016). Magnetic field evolution in magnetar crusts through three-dimensional simulations. *Proc. Natl. Acad. Sci.* 113, 3944–3949. doi:10.1073/pnas.1522363113

Gullón, M., Pons, J. A., Miralles, J. A., Viganò, D., Rea, N., and Perna, R. (2015). Population synthesis of isolated neutron stars with magneto-rotational evolution - II. From radio-pulsars to magnetars. *MNRAS* 454, 615–625. doi:10.1093/mnras/stv1644

Harrison, F. A., Craig, W. W., Christensen, F. E., Hailey, C. J., Zhang, W. W., Boggs, S. E., et al. (2013). The nuclear spectroscopic telescope Array (NuSTAR) high-energy X-ray mission. *ApJ* 770, 103. doi:10.1088/0004-637X/770/2/103

Heger, A., Fryer, C. L., Woosley, S. E., Langer, N., and Hartmann, D. H. (2003). How massive single stars end their life. *ApJ* 591, 288–300. doi:10.1086/375341

Hu, K., Baring, M. G., Harding, A. K., and Wadiasingh, Z. (2022). High-energy photon opacity in the twisted magnetospheres of magnetars. *ApJ* 940, 91. doi:10.3847/1538-4357/ac9611

Hu, K., Baring, M. G., Wadiasingh, Z., and Harding, A. K. (2019). Opacities for photon splitting and pair creation in neutron star magnetospheres. *MNRAS* 486, 3327–3349. doi:10.1093/mnras/stz995

Jackson, M. S., and Halpern, J. P. (2005). A refined ephemeris and phase-resolved X-ray spectroscopy of the Geminga pulsar. *ApJ* 633, 1114–1125. doi:10.1086/491615

Jansen, F., Lumb, D., Altieri, B., Clavel, J., Ehle, M., Erd, C., et al. (2001). XMM-Newton observatory. I. The spacecraft and operations. *A&A* 365, L1–L6. doi:10.1051/0004-6361:20000036

Kaplan, D. L. (2008). "Nearby, thermally emitting neutron stars," in *Astrophysics of compact objects of American Institute of physics conference series*. Editors Y.-F. Yuan, X.-D. Li, and D. Lai, 968, 129–136. doi:10.1063/1.2840384

Kaspi, V. M., Archibald, R. F., Bhalerao, V., Dufour, F., Gotthelf, E. V., An, H., et al. (2014). Timing and flux evolution of the galactic center magnetar SGR j1745-2900. *ApJ* 786, 84. doi:10.1088/0004-637X/786/2/84

Kaspi, V. M., and Beloborodov, A. M. (2017). Magnetars. *ARAA* 55, 261–301. doi:10.1146/annurev-astro-081915-023329

Kaspi, V. M., and Boydstun, K. (2010). On the X-ray spectra of anomalous X-ray pulsars and soft gamma repeaters. *ApJL* 710, L115–L120. doi:10.1088/2041-8205/710/2/L115

Kaspi, V. M., Gavriil, F. P., Woods, P. M., Jensen, J. B., Roberts, M. S. E., and Chakrabarty, D. (2003). A major soft gamma repeater-like outburst and rotation glitch in the No-longer-so-anomalous X-ray pulsar 1E 2259+586. *ApJL* 588, L93–L96. doi:10.1086/375683

Kirsten, F., Snelders, M. P., Jenkins, M., Nimmo, K., van den Eijnden, J., Hessels, J. W. T., et al. (2020). Detection of two bright radio bursts from magnetar SGR 1935 + 2154. *Nat. Astron.* 5, 414–422. doi:10.1038/s41550-020-01246-3

Kouveliotou, C., Dieters, S., Strohmayer, T., van Paradijs, J., Fishman, G. J., Meegan, C. A., et al. (1998). An X-ray pulsar with a superstrong magnetic field in the soft γ-ray repeater SGR1806 - 20. *Nature* 393, 235–237. doi:10.1038/30410

Kouveliotou, C., Strohmayer, T., Hurley, K., van Paradijs, J., Finger, M. H., Dieters, S., et al. (1999). Discovery of a magnetar associated with the soft gamma repeater SGR 1900+14. *ApJL* 510, L115–L118. doi:10.1086/311813

Kouveliotou, C., Woosley, S. E., Patel, S. K., Levan, A., Blandford, R., Ramirez-Ruiz, E., et al. (2004). Chandra observations of the X-ray environs of SN 1998bw/GRB 980425. *ApJ* 608, 872–882. doi:10.1086/420878

Kuiper, L., Hermsen, W., den Hartog, P. R., and Collmar, W. (2006). Discovery of luminous pulsed hard X-ray emission from anomalous X-ray pulsars 1RXS j1708-4009, 4U 0142+61, and 1E 2259+586 by INTEGRAL and RXTE. *ApJ* 645, 556–575. doi:10.1086/504317

Kuiper, L., Hermsen, W., and Mendez, M. (2004). Discovery of hard nonthermal pulsed X-ray emission from the anomalous X-ray pulsar 1E 1841-045. *ApJ* 613, 1173–1178. doi:10.1086/423129

Lander, S. K. (2023). The game of life on a magnetar crust: from gamma-ray flares to FRBs. *ApJL* 947, L16. doi:10.3847/2041-8213/acca1f

Lander, S. K., Andersson, N., Antonopoulou, D., and Watts, A. L. (2015). Magnetically driven crustquakes in neutron stars. *MNRAS* 449, 2047–2058. doi:10.1093/mnras/stv432

Lander, S. K., and Gourgouliatos, K. N. (2019). Magnetic-field evolution in a plastically failing neutron-star crust. *MNRAS* 486, 4130–4143. doi:10.1093/mnras/stz1042

Li, C. K., Lin, L., Xiong, S. L., Ge, M. Y., Li, X. B., Li, T. P., et al. (2021). HXMT identification of a non-thermal X-ray burst from SGR J1935+2154 and with FRB 200428. *Nat. Astron.* 5, 378–384. doi:10.1038/s41550-021-01302-6

Lien, A., Sakamoto, T., Barthelmy, S. D., Baumgartner, W. H., Cannizzo, J. K., Chen, K., et al. (2016). The third Swift burst alert telescope gamma-ray burst catalog. *ApJ* 829, 7. doi:10.3847/0004-637X/829/1/7

Lin, L., Göğüş, E., Roberts, O. J., Baring, M. G., Kouveliotou, C., Kaneko, Y., et al. (2020a). Fermi/GBM view of the 2019 and 2020 burst active episodes of SGR J1935+2154. *ApJL* 902, L43. doi:10.3847/2041-8213/abbefe

Lin, L., Zhang, C. F., Wang, P., Gao, H., Guan, X., Han, J. L., et al. (2020b). No pulsed radio emission during a bursting phase of a Galactic magnetar. *Nature* 587, 63–65. doi:10.1038/s41586-020-2839-y

Lorimer, D. R., Bailes, M., McLaughlin, M. A., Narkevic, D. J., and Crawford, F. (2007). A bright millisecond radio burst of extragalactic origin. *Science* 318, 777–780. doi:10.1126/science.1147532

Madsen, K. K., Reynolds, S., Harrison, F., An, H., Boggs, S., Christensen, F. E., et al. (2015). Broadband X-ray imaging and spectroscopy of the Crab nebula and pulsar with NuSTAR. *ApJ* 801, 66. doi:10.1088/0004-637X/801/1/66

Madsen, K. K., García, J. A., Stern, D., Armini, R., Basso, S., Coutinho, D., et al. (2023). The high energy x-ray probe (HEX-P): instrument and mission profile. *arXiv*. doi:10.48550/arXiv.2312.04678

Mahlmann, J. F., Philippov, A. A., Levinson, A., Spitkovsky, A., and Hakobyan, H. (2022). Electromagnetic fireworks: fast radio bursts from rapid reconnection in the compressed magnetar wind. *ApJL* 932, L20. doi:10.3847/2041-8213/ac7156

Manchester, R. N., Hobbs, G. B., Teoh, A., and Hobbs, M. (2005). The Australia telescope national facility pulsar catalogue. *AJ* 129, 1993–2006. doi:10.1086/428488

Marsden, D., and White, N. E. (2001). Correlations between spectral properties and spin-down rate in soft gamma-ray repeaters and anomalous X-ray pulsars. *ApJL* 551, L155–L158. doi:10.1086/320025

Maruyama, T., Balantekin, A. B., Cheoun, M.-K., Kajino, T., and Mathews, G. J. (2018). Axion production from Landau quantization in the strong magnetic field of magnetars. *Phys. Lett. B* 779, 160–165. doi:10.1016/j.physletb.2018.01.084

Meegan, C., Lichti, G., Bhat, P. N., Bissaldi, E., Briggs, M. S., Connaughton, V., et al. (2009). The *fermi*gamma-ray burst monitor. *ApJ* 702, 791–804. doi:10.1088/0004-637X/702/1/791

Meidinger, N., Albrecht, S., Beitler, C., Bonholzer, M., Emberger, V., Frank, J., et al. (2020). "Development status of the wide field imager instrument for Athena," in *Society of photo-optical instrumentation engineers (SPIE) conference series*, 11444, 114440T. doi:10.1117/12.2560507

Mereghetti, S., Savchenko, V., Ferrigno, C., Götz, D., Rigoselli, M., Tiengo, A., et al. (2020). INTEGRAL discovery of a burst with associated radio emission from the magnetar SGR 1935+2154. *ApJL* 898, L29. doi:10.3847/2041-8213/aba2cf

Mori, K., Gotthelf, E. V., Dufour, F., Kaspi, V. M., Halpern, J. P., Beloborodov, A. M., et al. (2014). A broadband X-ray study of the Geminga pulsar with NuSTAR and XMM-Newton. *ApJ* 793, 88. doi:10.1088/0004-637X/793/2/88

Nandra, K., Barret, D., Barcons, X., Fabian, A., den Herder, J.-W., Piro, L., et al. (2013). The hot and energetic universe: a white paper presenting the science theme motivating the Athena+ mission. arXiv e-prints, arXiv:1306.2307 Available at: https://arxiv.org/abs/1306.2307.

Olausen, S. A., and Kaspi, V. M. (2014). The McGill magnetar catalog. *ApJS* 212, 6. doi:10.1088/0067-0049/212/1/6

Parfrey, K., Beloborodov, A. M., and Hui, L. (2013). Dynamics of strongly twisted relativistic magnetospheres. *ApJ* 774, 92. doi:10.1088/0004-637X/774/2/92

Park, S., Bhalerao, J., Kargaltsev, O., and Slane, P. O. (2020). NuSTAR detection of quiescent hard X-ray emission from SGR 0526-66 in the large magellanic Cloud. *ApJ* 894, 17. doi:10.3847/1538-4357/ab83f8

Petroff, E., Hessels, J. W. T., and Lorimer, D. R. (2022). Fast radio bursts at the dawn of the 2020s. *AAPR* 30, 2. doi:10.1007/s00159-022-00139-w

Philippov, A., and Kramer, M. (2022). Pulsar magnetospheres and their radiation. *ARAA* 60, 495–558. doi:10.1146/annurev-astro-052920-112338

Pires, A. M., Schwope, A. D., and Motch, C. (2017). Follow-up of isolated neutron star candidates from the eROSITA survey. *Astron. Nachrichten* 338, 213–219. doi:10.1002/asna.201713333

Platts, E., Weltman, A., Walters, A., Tendulkar, S. P., Gordin, J. E. B., and Kandhai, S. (2019). A living theory catalogue for fast radio bursts. *Phys. Rep.* 821, 1–27. doi:10.1016/j.physrep.2019.06.003

Pons, J. A., and Rea, N. (2012). Modeling magnetar outbursts: flux enhancements and the connection with short bursts and glitches. *ApJL* 750, L6. doi:10.1088/2041-8205/750/1/L6

Predehl, P., Andritschke, R., Arefiev, V., Babyshkin, V., Batanov, O., Becker, W., et al. (2021). The eROSITA X-ray telescope on SRG. *A&A* 647, A1. doi:10.1051/0004-6361/202039313

Rea, N., Borghese, A., Esposito, P., Coti Zelati, F., Bachetti, M., Israel, G. L., et al. (2016). Magnetar-like activity from the central compact object in the SNR RCW103. *ApJL* 828, L13. doi:10.3847/2041-8205/828/1/L13

Rea, N., Coti Zelati, F., Dehman, C., Hurley-Walker, N., de Martino, D., Bahramian, A., et al. (2022). Constraining the nature of the 18 min periodic radio transient GLEAM-X j162759.5-523504.3 via multiwavelength observations and magneto-thermal simulations. *ApJ* 940, 72. doi:10.3847/1538-4357/ac97ea

Rea, N., Coti Zelati, F., Viganò, D., Papitto, A., Baganoff, F., Borghese, A., et al. (2020). The X-ray outburst of the galactic center magnetar over six years of Chandra observations. *ApJ* 894, 159. doi:10.3847/1538-4357/ab8387

Rea, N., Esposito, P., Turolla, R., Israel, G. L., Zane, S., Stella, L., et al. (2010). A low-magnetic-field soft gamma repeater. *Science* 330, 944–946. doi:10.1126/science.1196088

Rea, N., Israel, G. L., Turolla, R., Esposito, P., Mereghetti, S., Götz, D., et al. (2009). The first outburst of the new magnetar candidate SGR0501+4516. *MNRAS* 396, 2419–2432. doi:10.1111/j.1365-2966.2009.14920.x

Ridnaia, A., Svinkin, D., Frederiks, D., Bykov, A., Popov, S., Aptekar, R., et al. (2021). A peculiar hard X-ray counterpart of a Galactic fast radio burst. *Nat. Astron.* 5, 372–377. doi:10.1038/s41550-020-01265-0

Rigoselli, M., Mereghetti, S., Suleimanov, V., Potekhin, A. Y., Turolla, R., Taverna, R., et al. (2019). XMM-Newton observations of PSR J0726-2612, a radio-loud XDINS. *A&A* 627, A69. doi:10.1051/0004-6361/201935485

Seo, J., Lee, J., and An, H. (2023). Correlation study of temporal and emission properties of quiescent magnetars. *J. Korean Astronomical Soc.* 56, 41–57. doi:10.5303/JKAS.2023.56.1.41

Tan, C. M., Bassa, C. G., Cooper, S., Dijkema, T. J., Esposito, P., Hessels, J. W. T., et al. (2018). LOFAR discovery of a 23.5 s radio pulsar. *ApJ* 866, 54. doi:10.3847/1538-4357/aade88

Taverna, R., Turolla, R., Muleri, F., Heyl, J., Zane, S., Baldini, L., et al. (2022). Polarized x-rays from a magnetar. *Science* 378, 646–650. doi:10.1126/science.add0080

Taverna, R., Turolla, R., Suleimanov, V., Potekhin, A. Y., and Zane, S. (2020). X-ray spectra and polarization from magnetar candidates. *MNRAS* 492, 5057–5074. doi:10.1093/mnras/staa204

Thompson, C., and Duncan, R. C. (1995). The soft gamma repeaters as very strongly magnetized neutron stars - I. Radiative mechanism for outbursts. *MNRAS* 275, 255–300. doi:10.1093/mnras/275.2.255

van der Horst, A. J., Kouveliotou, C., Gorgone, N. M., Kaneko, Y., Baring, M. G., Guiriec, S., et al. (2012). SGR J1550–5418 bursts detected with the *fermi* gamma-ray burst monitor during its most prolific activity. *ApJ* 749, 122. doi:10.1088/0004-637X/749/2/122

Vasisht, G., and Gotthelf, E. V. (1997). The discovery of an anomalous X-ray pulsar in the supernova remnant K[CLC]es 73[/CLC]. *ApJL* 486, L129–L132. doi:10.1086/310843

Viganò, D., Rea, N., Pons, J. A., Perna, R., Aguilera, D. N., and Miralles, J. A. (2013). Unifying the observational diversity of isolated neutron stars via

magneto-thermal evolution models. *Mon. Notices R. Astronomical Soc.* 434, 123–141. doi:10.1093/mnras/stt1008

Wadiasingh, Z., Baring, M., Hu, K., Harding, A., Younes, G., and Gonthier, P. (2022). Phase-resolved spectropolarimetric models of magnetar hard X-ray emission with QED photon splitting attenuation. *AAS/High Energy Astrophys. Div.* 54, 47.

Wadiasingh, Z., Baring, M. G., Gonthier, P. L., and Harding, A. K. (2018). Resonant inverse Compton scattering spectra from highly magnetized neutron stars. *ApJ* 854, 98. doi:10.3847/1538-4357/aaa460

Wadiasingh, Z., and Timokhin, A. (2019). Repeating fast radio bursts from magnetars with low magnetospheric twist. *ApJ* 879, 4. doi:10.3847/1538-4357/ab2240

Wadiasingh, Z., Younes, G., Baring, M. G., Harding, A. K., Gonthier, P. L., Hu, K., et al. (2019). Magnetars as astrophysical laboratories of extreme quantum electrodynamics: the case for a Compton telescope. *BAAS* 51, 292. doi:10.48550/arXiv.1903.05648

Younes, G., Baring, M. G., Kouveliotou, C., Arzoumanian, Z., Enoto, T., Doty, J., et al. (2021). Broadband X-ray burst spectroscopy of the fast-radio-burst-emitting Galactic magnetar. *Nat. Astron.* 5, 408–413. doi:10.1038/s41550-020-01292-x

Younes, G., Güver, T., Kouveliotou, C., Baring, M. G., Hu, C.-P., Wadiasingh, Z., et al. (2020). NICER view of the 2020 burst storm and persistent emission of SGR 1935+2154. *ApJL* 904, L21. doi:10.3847/2041-8213/abc94c

Younes, G., Kouveliotou, C., Kargaltsev, O., Gill, R., Granot, J., Watts, A. L., et al. (2016). The wind nebula around magnetar Swift j1834.9-0846. *ApJ* 824, 138. doi:10.3847/0004-637X/824/2/138

Yuan, Y., Beloborodov, A. M., Chen, A. Y., and Levin, Y. (2020). Plasmoid ejection by alfvén waves and the fast radio bursts from SGR 1935+2154. *ApJL* 900, L21. doi:10.3847/2041-8213/abafa8

Zane, S., Taverna, R., González-Caniulef, D., Muleri, F., Turolla, R., Heyl, J., et al. (2023). A strong X-ray polarization signal from the magnetar 1RXS j170849.0-400910. *ApJL* 944, L27. doi:10.3847/2041-8213/acb703

Zhang, B. (2023). The physics of fast radio bursts. *Rev. Mod. Phys.* 95, 035005. doi:10.1103/RevModPhys.95.035005

Zhang, W., Basu-Zych, A., Bautz, M., Brandt, W., Cenko, S., Chan, K.-W., et al. (2022). The survey and time-domain astrophysical research explorer (STAR-X). *AAS/High Energy Astrophys. Div.* 54, 45.